Celal Bayar University Journal of Science

# Prediction of Earthquake Magnitude Using Tree-Based Ensemble Learning

Selin Erzin[1]*, Can Saç[2]

[1] Dokuz Eylul University, Science Faculty, Physics Department, 35390 İzmir, Türkiye.
[2] Eastern Mediterranean University, Medicine Faculty, 99628 Famagusta, North Cyprus.
* selin.erzin@deu.edu.tr
* Orcid No: 0000-0001-8885-4251

Received: June 30, 2025
Accepted: August 23, 2025
DOI: 10.18466/cbayarfbe.1730783

**Abstract**

The present paper aims at predicting earthquake magnitude ($M_w$) from soil gas radon concentration ($C_{Rn}$) and three meteorological parameters (hourly humidity ($H$), hourly temperature ($T$), and hourly air pressure ($P$)). To accomplish this, three tree-based ensemble machine learning approaches, namely gradient boosting (GBoost), extreme gradient boosting (XGBoost), and random forest (RF), were created. A total of 386 datasets including recorded $M_w$ values and measured soil gas $C_{Rn}$, $H$, $T$, and $P$ values were used to develop the models. The models were then verified using statistics such as relative absolute error (*RAE*), root mean square error (*RMSE*), mean absolute error (*MAE*), and the ratio of *RMSE* to data standard deviation (*RSR*). A comparison of the performance metrics reveals that the GBoost model predicted the $M_w$ value with lower *MAE*, *RMSE*, *RSR*, and *RAE* values than both the XGBoost and RF models. Performance was also verified using rank analysis and plots of Taylor and scaled percentage error (*SPE*). Rank analysis showed that the GBoost model received higher overall scores than both the XGBoost and RF models, indicating that the GBoost model achieved better prediction accuracy than both the XGBoost and RF models in predicting the Mw values. Both Taylor and *SPE* plots showed that GBoost model predicted the $M_w$ values more accurately than XGBoost and RF models. According to the results of the study, the GBoost model can be used to predict $M_w$ reliably and quickly, provided that three meteorological factors ($H$, $T$, and $P$) and soil gas $C_{Rn}$ values are available.

**Keywords:** Earthquake magnitude, Soil gas radon concentration, Extreme gradient boosting, Gradient boosting, Random forest.

## 1. Introduction

Earthquakes are one of the most damaging and life-destroying natural hazards that occur as a result of energy released from the Earth's crust [1]. Earthquakes can cause major loss of life and property, thus early preparation for these risks is an important aspect in reducing their damage and consequences. Earthquakes are difficult to forecast, and many scientists have long been interested in predicting them [2, 3]. Many parameters are being studied around the world to predict the location, time and intensity of possible earthquakes. One of the parameters emphasized in these studies is the relationship between soil gas radon anomalies and seismic activities.

Radon is a naturally occurring, colourless, and odourless radioactive gas made up of three isotopes: $^{219}$Rn, $^{220}$Rn, and $^{222}$Rn [4, 5]. The $^{222}$Rn isotope is a byproduct of uranium and has a longer life than the other two isotopes. The total amount of natural $^{222}$Rn is also much greater than that of natural $^{219}$Rn and $^{220}$Rn. Therefore, the name "radon" is used to refer to $^{222}$Rn in most studies, including this one. Radon gas is present in the atmosphere in varying concentrations. Although the amount of radon created in rocks and soils relies on their uranium level, radon concentration ($C_{Rn}$) comes from water, soil, and air [4, 5]. Seismic activity can cause radon to rise due to decompression and compression in the Earth's crust's upper layer [1]. Measuring variations in radon levels in soil and groundwater before and after crustal movement is a useful tool for tracking stress changes caused by seismic activity and is therefore an important parameter to understand for radon monitoring [6].

Several research studies have been conducted to monitor and assess the soil radon levels in connection with seismic activity. These studies indicate that the soil radon levels can provide useful information for analyzing the earth's crust's tectonic activity, as earthquakes can cause significant variations in soil radon levels [7, 8]. Several researchers [9-12] have shown that radon levels in fault zones increase from a few hours to several weeks before earthquakes occur. Abnormal radon changes before earthquakes have been found in groundwater, soil gas, atmosphere, and thermal spas [13-22]. Several researchers [1, 23-26] have also suggested that radon anomalies can be used to identify earthquake precursors.

Gradient boosting (GBoost), extreme gradient boosting (XGBoost) and random forest (RF) are popular tree-based ensemble machine learning (ML) techniques utilized for regression and classification tasks. GBoost creates a powerful prediction model by combining several weaker models′ predictions [27]. GBoost accomplishes this by continuously training new models to correct the previous ones' errors [28]. XGBoost is an optimisation of GBoost combining techniques of regularization for both preventing model over-fitting and improving its generalization [29]. XGBoost excels at handling massive datasets and is versatile enough for a variety of applications [28]. RF is an integrated approach that designs multiple decision trees (DTs) for simultaneous training and uses the average of the predictions as output [30]. The randomization involved in feature and sample selection helps to prevent over-fitting, making RF a viable option for many classification and regression applications.

Considering the advantage of tree-based ensemble ML techniques, three tree-based ensemble ML models (GBoost, XGBoost and RF) were developed in this study to predict earthquake magnitude ($M_w$) from soil gas $C_{Rn}$ and three meteorological parameters, namely hourly humidity ($H$), hourly temperature ($T$), and hourly air pressure ($P$). To achieve this, firstly, soil gas $C_{Rn}$ measurements were conducted at a randomly selected site in the Seferihisar district of İzmir, where the earthquake risk is high and the fault lines are located. Secondly, the measurements of three meteorological parameters ($H$, $T$, and $P$) in the study area were obtained from the Ministry of Agriculture and Forestry of the Republic of Turkey, General Directorate of Meteorology. Thirdly, the $M_w$ values recorded in the study area during the study period were obtained from the Kandilli Observatory of Boğaziçi University and the Seismology Laboratory of the Earthquake Research Institute. The predicted $M_w$ values from the GBoost, XGBoost and RF models were compared with the $M_w$ values recorded in the study area. Furthermore, the predictive abilities of the GBoost, XGBoost and RF models were assessed using a variety of performance metrics, including relative absolute error (*RAE*), root mean square error (*RMSE*), mean absolute error (*MAE*), and ratio of *RMSE* to data standard deviation (*RSR*). Comparison of the performance metrics shows that the GBoost model predicted the $M_w$ value with lower *RAE*, *RMSE*, *MAE*, and *RSR* values than both the XGBoost and RF models. The performance of the GBoost, XGBoost and RF models was further verified by rank analysis and visual interpretation using Taylor and scaled percentage error (*SPE*) graphs. Rank analysis showed that the GBoost model received higher overall scores than both the XGBoost and RF models, indicating that the GBoost model achieved better prediction accurately than both the XGBoost and RF models in the prediction of $M_w$ values. Taylor and *SPE* graphs showed that the GBoost model predicted the $M_w$ values more precisely than the XGBoost and RF models.

## 2. Materials and Methods

### 2.1. Study area

Türkiye, one of the most seismically active countries in the world, is located in the active Alpine-Himalayan seismic zone, where 20% of the world's earthquakes occur, with one damaging earthquake occurring in Türkiye each 5 years [31]. Approximately 95% of the Turkish population is at risk from earthquakes, according to the Turkish Earthquake Code 2018 [32] Seferihisar region of Izmir is one of the regions where seismic activity is intense. Earthquakes have occurred continuously since the past. The most recent earthquake with a $M_w$ of 6.9 that occurred in the region on October 30, 2020, affected the Bayraklı district of Izmir and caused many casualties. In addition, data on the tsunami caused by the earthquake in the region were collected during field observations made in Seferihisar on October 30-31 and November 1, 2020. Changes in sea level were observed at the moment of the earthquake, before and after. According to eyewitness accounts, sea retreat was observed at levels of 100-200 meters.

### 2.2. Radon measurements in soil

Digital radon detector was placed in a small container next to the garden wall of a house in the Seferihisar district of Izmir. This small chamber, with a side of 50 cm, was placed in the soil. A 30 cm funnel was placed on the floor of the chamber. The detector was mounted at the mouth of the funnel. This way, air from the soil reaches the detector directly. The system was regularly checked. Soil gas $C_{Rn}$ measurements were conducted at recorded intervals between 2 August 2021 and 30 December 2021.

### 2.3. Tree-based ensemble ML techniques

#### 2.3.1. Gradient boosting (GBoost)

Boosting algorithms develop strong learners by repeatedly combining weak learners (those that are marginally better than random) [33]. GBoost is a

boosting technique for regression [30] and a complicated ensemble ML technique that has become popular because of its great precision and persistence in prediction. GBoost continually creates DTs, with each new tree improving on the faults committed by previous ones [34, 35]. This iterative process, reducing the loss function of the model, is based on the optimization technique of gradient descent [36]. The primary aim is to achieve weak models′ optimal combination to produce a very accurate and reliable prediction [36]. GBoost can manage intricate and nonlinear correlations between input variables and the target variable, making it especially useful in circumstances where traditional linear regression models may not be sufficient [36]. In addition, GBoost performs well with minimal training data, which decreases the overfitting risk [36]. Furthermore, GBoost can deal with a wide range of data formats, such as numeric, categoric and absent values. Its adaptability allows it to handle diverse real data sets with different characteristics [34, 37].

#### 2.3.2. Extreme gradient boosting (XGBoost)

XGBoost is a distinctive and significant ensemble ML algorithm based on GBoost DTs that has received considerable attention in recent years. When dealing with large numbers of datasets with various features and observations, XGBoost stands out for its remarkable speed, scaling and efficiency [36]. XGBoost also outperforms existent techniques in terms of training and prediction by using parallel computation and state-of-the-art algorithms [36]. In addition, XGBoost applies both L1 and L2 regularisation, which helps to prevent overfitting and enhance model performance, especially on complex datasets. Furthermore, XGBoost has a built-in support for missing values, which makes data preparation easier and more robust [38]. It uses a unique tree-pruning strategy to minimize model complexity by continually removing uninteresting splits, enhancing interpretability, and lowering the overfitting risk [36]. XGBoost's ability to capture complex nonlinear relationships in the data set and provide stable prediction performance by building multiple DTs and integrating their predictions makes it suitable for a wide range of applications, including the solution of ranking, classification, regression, and custom prediction problems [39]. In general, XGBoost is a remarkable and reliable ML technique that enables data scientists and practitioners to work in a variety of fields, thanks to its combination of speed, regularization capability, missing value handling, tree pruning, nonlinear modelling, understanding and diversity [40-42].

#### 2.3.3. Random forest (RF)

RF is a frequently employed, computationally efficient ensemble ML technique for many classification, regression and feature selection applications due to its fast processing, high model performance and simple parameter optimization techniques [43]. The basic concept of RF is to use DTs as the fundamental building block, and to take k sets of training data from the source dataset by random and replacement sampling methods [44]. The samples taken on each set are not completely consistent [44]. For each k training set, DTs are constructed based on specified criteria to produce the results of the regression [44]. Finally, the average of the estimated results is computed to obtain a final result. The constructed DTs possess a high degree of randomness and are capable of fitting numerous nonlinear relations, whilst overfitting is being controlled to prevent the fitting ability from increasing indefinitely, which improves the random forest's accuracy and generalizability [44]. The RF model surpasses support vector machines and neural networks in terms of accuracy and robustness [44].

## 3. Research Methodology

The current study applies and evaluates RF, GBoost and XGBoost models to predict the $M_w$ values from soil gas $C_{Rn}$ and three meteorological properties ($T$, $P$, and $H$). To achieve this, a total of 386 data sets including recorded $M_w$ values and measured soil gas $C_{Rn}$, $H$, $T$, and $P$ values in the study area were used to build, learn and analyze the RF, GBoost and XGBoost models. The models were first trained on randomly selected 80% of the data sets and then tested on the remaining 20%. Four performance indices (*RAE*, *RMSE*, *RSR* and *MAE*) were employed for evaluating GBoost, XGBoost and RF models′ performance during training and testing. The constructed models′ performance was further validated by rank analysis, visual interpretation using Taylor and scaled percentage error (*SPE*) plots and external validation. Figure 1 shows the methodology of this study.

## 4. Data Analysis and Development of RF, GBoost, and XGBoost models

### 4.1. Data Analysis

In the development of the RF, GBoost and XGBoost models, the soil gas $C_{Rn}$, $T$, $P$, and $H$ values were used as input parameters. In all models, the $M_w$ value was the only output parameter. Table 1 shows the descriptive statistics for each parameter used in the models. Figure 2 depicts a visual depiction of input and output parameters in the models, including histograms. As shown in Table 1, the standard deviations of the $T$, $H$, $P$, $C_{Rn}$, and $M_w$ parameters are smaller than their respective means, which indicates that their distribution among the considered samples is very homogeneous. In this study, the skewness and kurtosis coefficients were examined to assess the normality of the $T$, $H$, $P$, $C_{Rn}$, and $M_w$ parameters considered. The skewness and kurtosis coefficients show the form and symmetry (flat or peak) of the data [45]. The values of these coefficients might be undefined, positive, or negative [46]. A positive skewness indicates a distribution pattern that is skewed

to the right and a negative skewness indicates a distribution pattern that is skewed to the left [47]. A negative kurtosis indicates flatter data, and a positive kurtosis shows a peaked data plot [48, 49]. The skewness and kurtosis coefficients are both 0, suggesting the data follows a normal distribution, which is symmetric because the bulk of the data is close to the mean. These coefficients are rarely zero. Therefore, Bulmer [50], Tabachnick and Fidell [51], and Gravetter and Wallnau [52] recommended ranges of ±1, ±1.5, and ±2, respectively, for these coefficients. According to Bryne et al. [53] and Hair et al. [54], the normalcy assumption is not met when the skewness coefficient is more than ±2 and the kurtosis coefficient is greater than ±7. Table 1 illustrates that the skewness coefficients for the $T$, $H$, $P$, $C_{Rn}$ and $M_w$ variables were 0.54, -0.18, -0.70, 1.33 and 1.14 respectively, while their kurtosis coefficients were -1.14, -0.72, 1.48, 2.07 and 1.69, respectively. Thus, skewness and kurtosis for each variable are within acceptable ranges suggested by Bryne et al. [53] and Hair et al. [54], suggesting a normal distribution of each variable used in modelling.

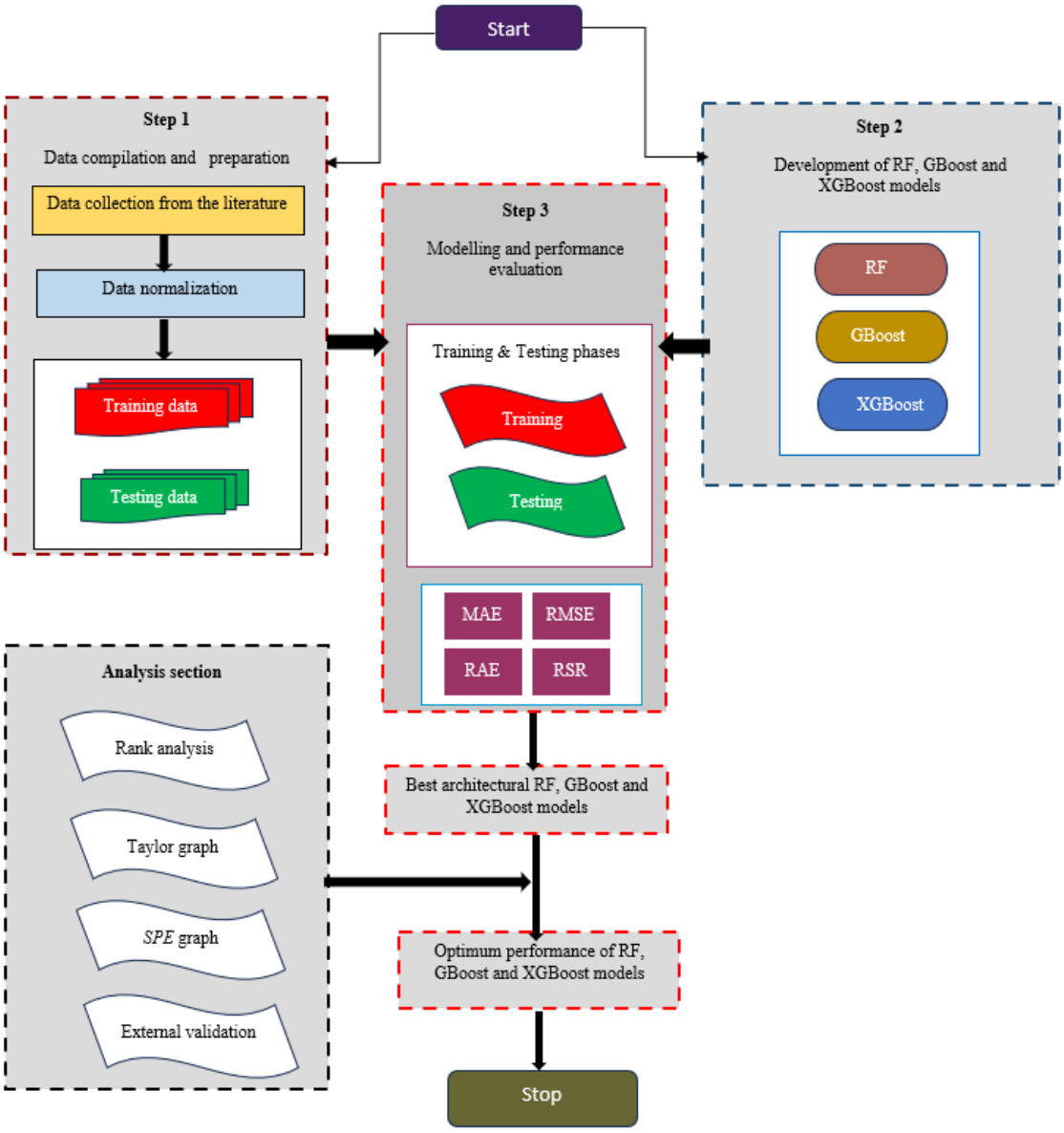



**Figure 1**. The methodology of this study.

Celal Bayar University Journal of Science
Volume 21, Issue 3, 2025, p 89-106
Doi: 10.18466/cbayarfbe.1730783


**Table 1**. The descriptive statistical values of the parameters used in the RF, GBoost, and XGBoost models.

| Parameters | $T$ (°C) | $H$ (%) | $P$ (hPa) | $C_{Rn}$ (Bq m$^{-3}$) | $M_w$ |
|---|---|---|---|---|---|
| Category | Input | Input | Input | Input | Output |
| $N$ total | 386 | 386 | 386 | 386 | 386 |
| Minimum | 27.10 | 47.70 | 999.10 | 16 | 1.00 |
| Maximum | 29.80 | 61.00 | 1014.70 | 455 | 3.80 |
| Mean | 28.25 | 55.56 | 1008.23 | 99.81 | 1.65 |
| Median | 27.80 | 55.75 | 1008.50 | 79.40 | 1.60 |
| Standard deviation | 0.85 | 2.99 | 2.84 | 76,71 | 0.48 |
| Skewness | 0.54 | -0.18 | -0.70 | 1.33 | 1.14 |
| Kurtosis | -1.14 | -0.72 | 1.48 | 2.07 | 1.69 |

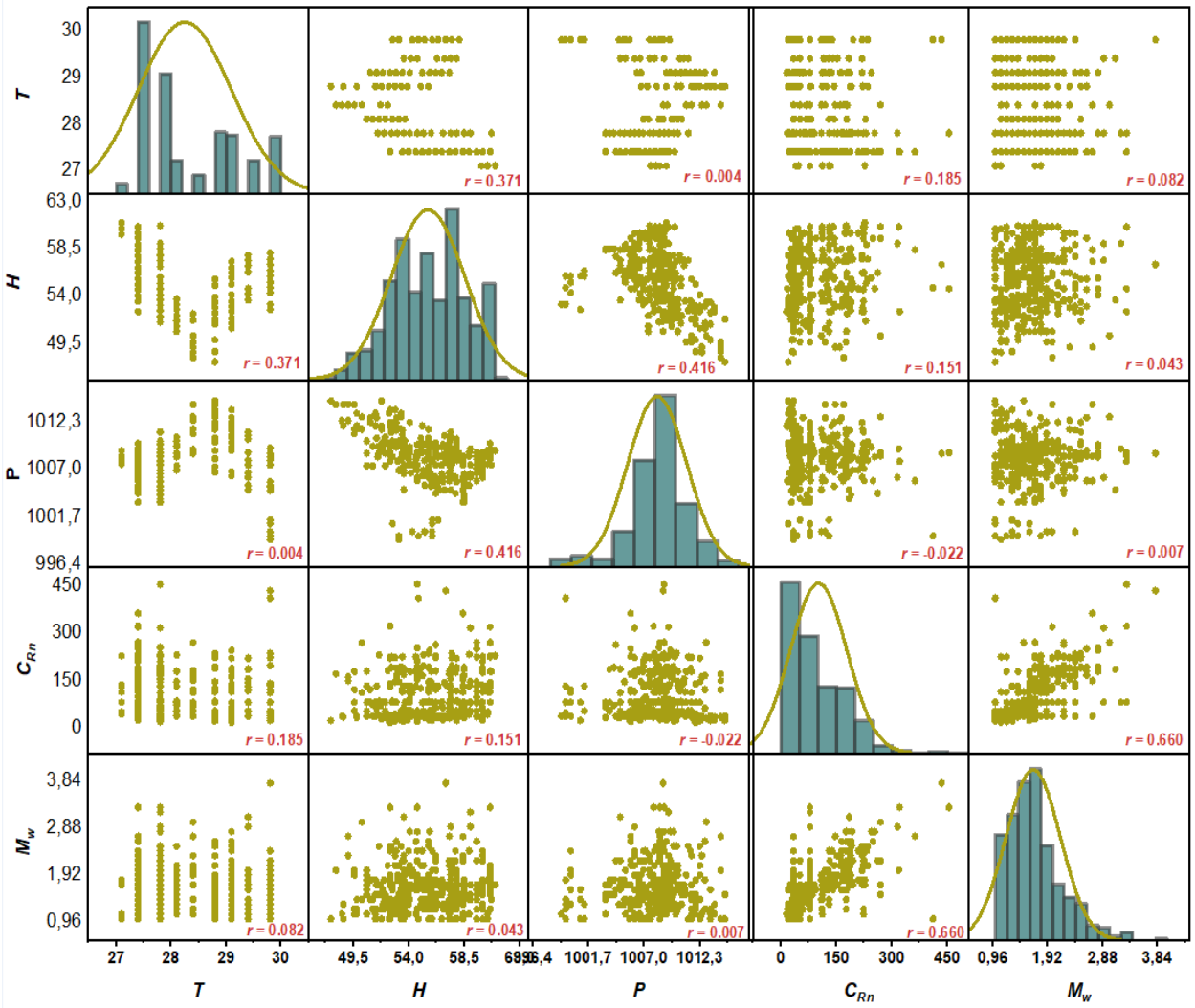



**Figure 2**. A graphical representation with histograms of input and output parameters in RF, GBoost, and XGBoost models.

The Pearson correlation ($r$) measures how strongly a linear correlation is present between the variables in question. The correlation within variables according to $r$ value range is given in Table 2. The $r$ value computed for each input parameter ($T$, $P$, $H$, and $C_{Rn}$) and output parameter ($M_w$) used in the models is also shown in Fig. 2. Based on the $r$ values mentioned in Table 2, $r$ value of 0.082 for $T$ and $M_w$, $r$ value of 0.043 for $H$ and $M_w$ and $r$ value of 0.007 for $P$ and $M_w$ indicates no relationship between each meteorological parameter and $M_w$; $r$ value of 0.660 for $C_{Rn}$ and $M_w$ indicates a strong relationship between $C_{Rn}$ and $M_w$.

**Table 2**. Level of relationship between variables based on the range of $r$ values [55].

| $r$ value | Level of relationship |
|---|---|
| ± 0.81 to ± 1.00 | Very strong/ Strongest |
| ± 0.61 to ± 0.80 | Strong |
| ± 0.41 to ± 0.60 | Moderate |
| ± 0.21 to ± 0.40 | Weak |
| ± 0.00 to ± 0.20 | No relationship |

Preparation of the data is crucial for ensuring that all variables receive equal attention during training, leading to faster learning results [56]. Normalising both input and output variables is critical for improving the speed and accuracy of soft computing (SC) models [57]. The data normalisation technique was applied with the minimum-maximum scaler for rescaling the parameters used in the models to a range between 0 and 1. In this study, as in previous studies [56, 58-63], a randomly selected 80% of the data sets (308 data sets) was then used to build and train the RF, GBoost and XGBoost models, and the remaining 20% (78 data sets) was used to test the models.

### 4.2. Development of RF, GBoost, and XGBoost models

In this study, RF, GBoost and XGBoost models were developed using the Konstanz Information Miner (KNIME) Analytics Platform (version 5.4.2), a Java-based end-to-end analysis tool that integrates, transforms, analyses and deploys data [64], to predict the $M_w$ value. For this purpose, the data sets including the measurements of soil gas $C_{Rn}$ and three meteorological parameters ($T$, $H$, and $P$) were used. The $T$, $H$, $P$, and $C_{Rn}$ values were used as input parameters in the RF, GBoost and XGBoost models. The recorded $M_w$ value was used as an output parameter for the models.

Tuning the hyperparameters of an ML algorithm is the main feature of model learning and the best way to implement it successfully [65]. Hyperparameter tuning mechanisms differ among ML algorithms due to the various types of hyperparameters, continuous, categorical, and discrete [66]. Grid search (GS) has been the existing standard for optimising parameters on ML over the last few decades, involving an extensive search of a manually determined hyperparameter space's subsets of the ML algorithm [67]. GS has now become the state of the art for hyperparameter optimization because of its execution simplicity, parallelizability, and durability in low-dimensional spaces [67]. GS is therefore the most widely used method for learning hyperparameter configuration spaces [68] to find the best parameters for each ML algorithm. In this study, a GS was performed using KNIME Analytics Platform (version 5.4.2) for hyperparameter tuning of the RF, GBoost and XGBoost models to optimise their performance according to the least mean square error (*MSE)*. Table 3 shows the hyperparameter ranges and the optimized values found by the GS for GBoost, XGBoost and RF models.

**Table 3**. The hyperparameter ranges and the optimized values found by the GS for GBoost, XGBoost, and RF models.

| Ensemble ML model | Hyperparameter | Range | Optimum value |
|---|---|---|---|
| RF | Max_depth | 1-15 | 12 |
| | Minimum node size | 1-15 | 1 |
| | Number of trees | 50-500 | 50 |
| GBoost | Max_ depth | 1-15 | 9 |
| | Number of trees | 50-500 | 150 |
| | Learning rate | 0.01-0.3 | 0.02 |
| XGBoost | Max_depth | 1-15 | 8 |
| | Child_weight | 0.2-2 | 0.2 |
| | Subsample | 0.1-1 | 0.9 |
| | Colsample bytree | 0.1-1 | 1.0 |
| | Learning rate | 0.01-1.0 | 1.0 |

The SC models′ performance is analysed using various performance metrics [69]. After training GBoost, XGBoost and RF models with the optimized parameters, the reliability of the models was evaluated and verified using four performance measures presented by Equations (1) to (4). In these equations, $N$ is the number of samples; $y_i$ is determined value; $\overline{y}$ is $y_i$ values′ mean value; $\hat{y}_i$ is predicted value. A SC model is deemed to be reliable if the values of *MAE*, *RMSE*, *RSR* and *RAE* are approaching zero.

$$MAE = \frac{1}{N}\sum_{i=1}^{N}|y_i - \hat{y}_i| \quad (1)$$

$$RMSE = \sqrt{\frac{1}{N}\sum_{i=1}^{N}(y_i - \hat{y}_i)^2} \quad (2)$$

$$RSR = \frac{RMSE}{\sqrt{\frac{1}{N}\sum_{i=1}^{N}(y_i - \overline{y})^2}} \quad (3)$$

$$RAE = \frac{\sum_{i=1}^{N}|y_i - \hat{y}_i|}{\sum_{i=1}^{N}|y_i - \overline{y}|} \quad (4)$$

## 5. Results and discussion

### 5.1. Simulation of results

A comparison of recorded and predicted $M_w$ values from the RF, GBoost and XGBoost models for training and test samples is shown in Figs. 3, 4 and 5, respectively. As shown in Fig. 3, the $M_w$ values recorded were mostly similar to those predicted by the RF model for samples of training and testing, having values of $r$ = 0.995 and 0.984, respectively. Figure 4 shows the mostly remarkable similarity of the $M_w$ values recorded to those predicted by the GBoost model for samples of training and testing, having values of $r$ = 0.999 and 0.986, respectively. Figure 5 shows a fairly good agreement between $M_w$ values determined and those predicted by the XGBoost model for samples of training and testing, having values of $r$ = 0.990 and 0.985, respectively. Figures 3 to 5 show that all the developed RF, GBoost and XGBoost models yielded values of $r > 0.8$ for both training and test samples, indicating a very strong correlation between the recorded and predicted $M_w$ values from the developed models, according to the $r$ values listed in Table 2. In other words, there is no substantial difference between the recorded and predicted $M_w$ values from the models.

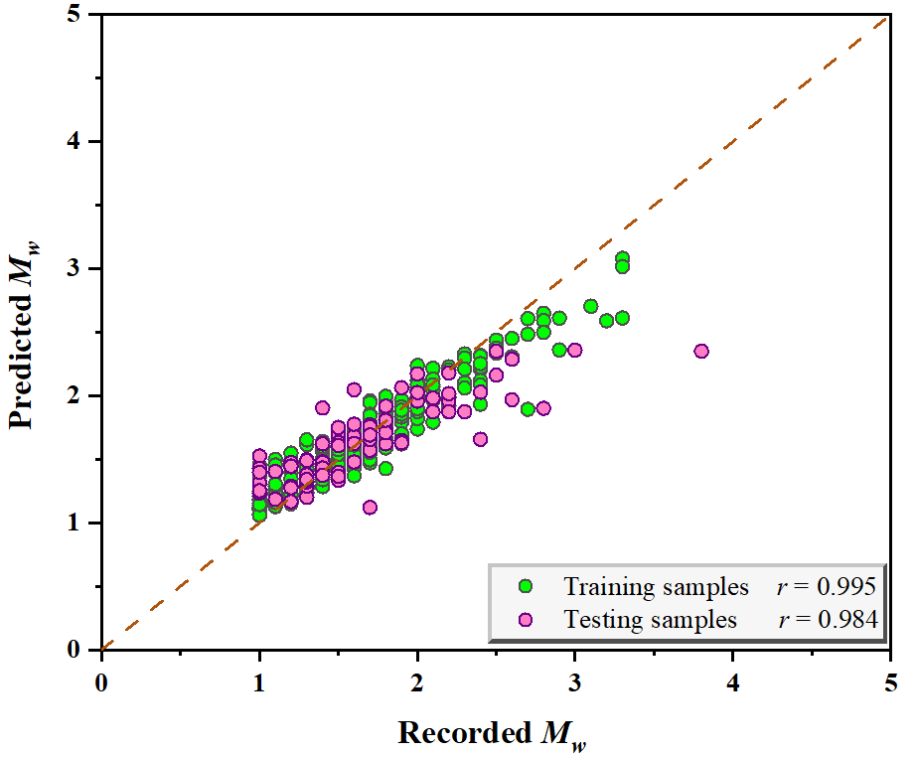



**Figure 3**. Comparison of the recorded and predicted $M_w$ values from the RF model for training and testing samples.

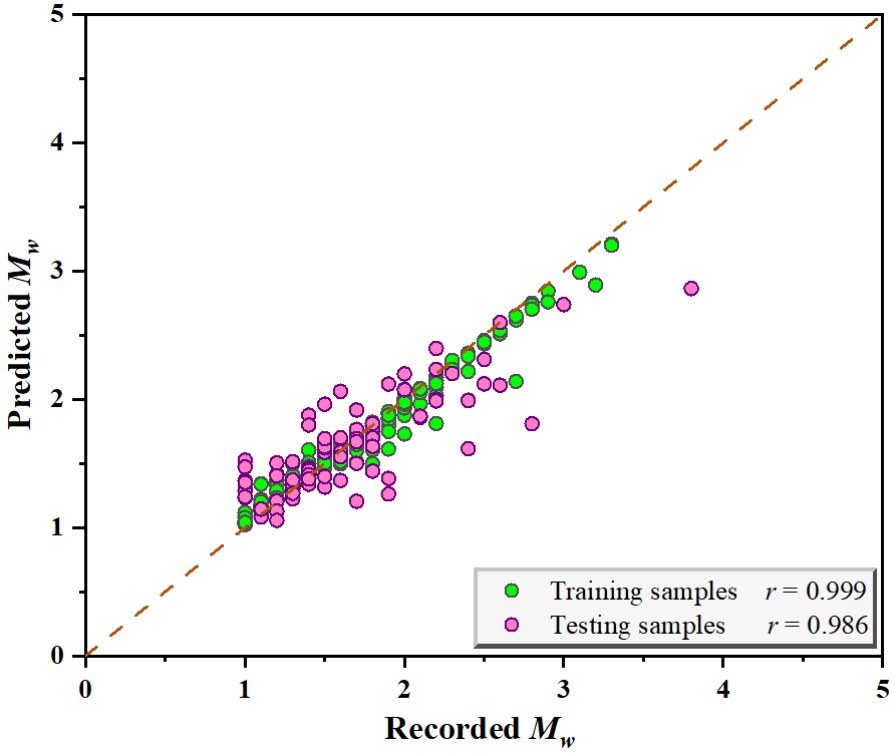



**Figure 4**. Comparison of the recorded and predicted $M_w$ values from the GBoost model for training and testing samples.

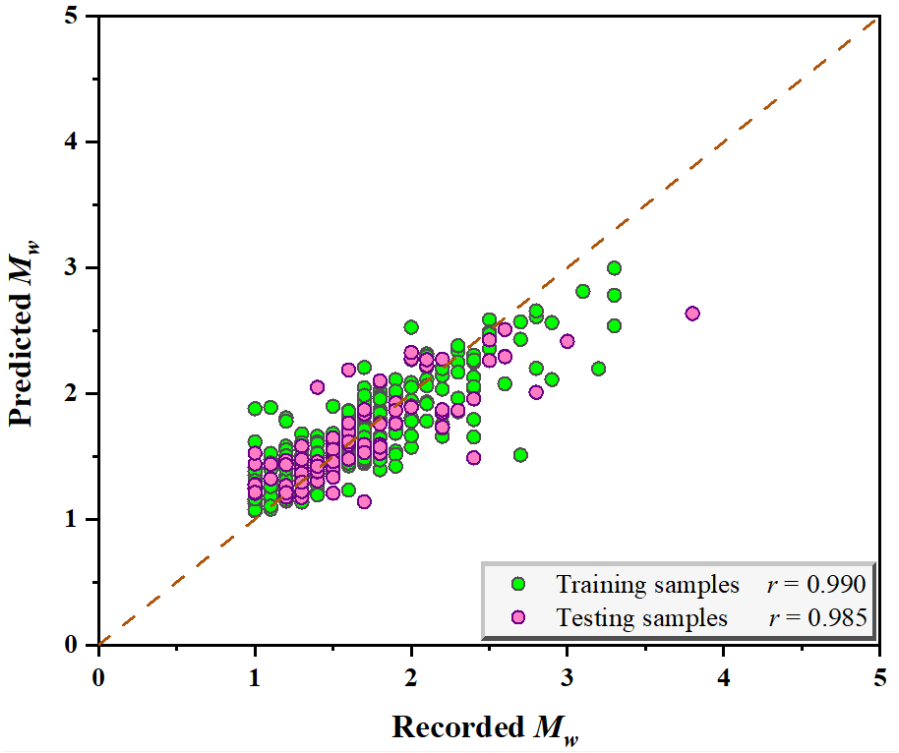



**Figure 5**. Comparison of recorded and predicted $M_w$ values from the XGBoost model for training and testing samples.

In reality, the $r$ value is a significant measure of the predictive ability of SC models. The performance of the models designed in this work was also assessed by four performance measures (*MAE*, *RMSE*, *RSR*, and *RAE*). The results are presented in Table 4 and also illustrated in Fig. 6. As shown in Fig. 6, the GBoost model achieved a better performance in predicting the $M_w$ value for both training and test samples compared to the RF and XGBoost models. The performance indices for the GBoost model in Fig. 6 also show that the $M_w$ value can be predicted reliably and quickly using the developed GBoost models, provided the values of soil gas $C_{Rn}$ and three meteorological parameters ($T$, $H$, and $P$) are available.

**Table 4**. Performance indices of the optimal RF, GBoost, and XGBoost models.

| Model | Data | *MAE* | *RMSE* | *RSR* | *RAE* |
|---|---|---|---|---|---|
| **RF** | Training set | 0.1189 | 0.1639 | 0.3523 | 0.3346 |
| | Testing set | 0.2207 | 0.3192 | 0.6139 | 0.8630 |
| **GBoost** | Training set | 0.0543 | 0.0859 | 0.1846 | 0.1529 |
| | Testing set | 0.2132 | 0.2983 | 0.5736 | 0.6831 |
| **XGBoost** | Training set | 0.1735 | 0.2439 | 0.5241 | 0.4881 |
| | Testing set | 0.2213 | 0.3080 | 0.5923 | 0.7092 |

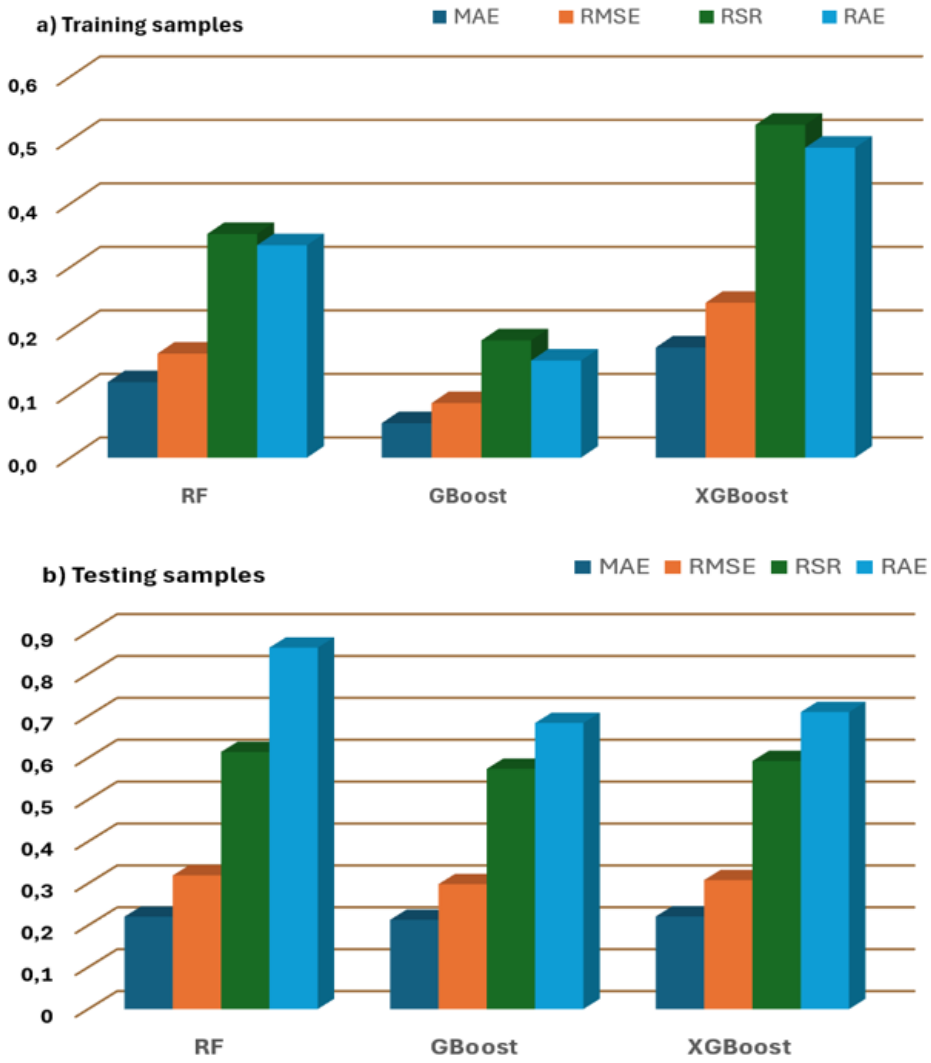



**Figure 6**. Performance indices of the optimal RF, GBoost, and XGBoost models.

### 5.2. Rank Analysis

Rank analysis is an easy and popular way to evaluate the performances of SC models [70, 71]. In the rank analysis, SC models are assessed on various performance metrics during the stages of training and testing [56]. The best model is ranked highest, the worst lowest, and the model with the highest score is selected as the best [72]. Different performance metrics were used in this study to determine the scores, with the optimal value of each metric used as a reference (see Table 5). Table 6 shows the ranking of the RF, GBoost and XGBoost models on the basis of the test and training performance metrics. As only three models were used, the highest score for a model in Table 6 is 3. Table 6 shows that the GBoost model scored higher (12 points) than the RF model (8 points) and the XGBoost model (4 points) for the training samples and scored higher (12 points) than the RF model (5 points) and the XGBoost model (7 points) for the test samples, indicating that the GBoost model outperforms both the RF and XGBoost models in predicting the $M_w$ value.

**Table 5**. Best values of performance metrics.

| Performance indices | Best value |
|---|---|
| *MAE* | 0 |
| *RMSE* | 0 |
| *RSR* | 0 |
| *RAE* | 0 |

**Table 6**. Rank analysis of the optimal RF, GBoost, and XGBoost models.

| | | Training | | | Testing | | |
|---|---|---|---|---|---|---|---|
| ***Parameters*** | **Value/Score** | RF | GBoost | XGBoost | RF | GBoost | XGBoost |
| ***MAE*** | Value | 0.1189 | 0.0543 | 0.1735 | 0.2207 | 0.2132 | 0.2213 |
| | Score | 2 | 3 | 1 | 2 | 3 | 1 |
| ***RMSE*** | Value | 0.1639 | 0.0859 | 0.2439 | 0.3192 | 0.2983 | 0.3080 |
| | Score | 2 | 3 | 1 | 1 | 3 | 2 |
| ***RSR*** | Value | 0.3523 | 0.1846 | 0.5241 | 0.6139 | 0.5736 | 0.5923 |
| | Score | 2 | 3 | 1 | 1 | 3 | 2 |
| ***RAE*** | Value | 0.3346 | 0.1529 | 0.4881 | 0.8630 | 0.6831 | 0.7092 |
| | Score | 2 | 3 | 1 | 1 | 3 | 2 |
| **Total** | | 8 | 12 | 4 | 5 | 12 | 7 |

### 5.3. Taylor graph

A simple visual representation of how SC model predictions relate to observations is also provided by Taylor graphs [73]. The graphs provide several statistical measures, such as *r*, centered *RMS* difference and standard deviation ratio to statistically compare the SC models′ performance [72]. Performance and competence of the proposed SC models are assessed against a reference value by using Taylor graphs [72]. The SC model whose position is most proximate to the reference point is selected as the optimum SC model [73]. Figure 7 shows the Taylor graph of the RF, GBoost and XGBoost models developed. As shown in Fig. 7, the marker position of the GBoost model is closer to the "reference" point than the positions of the RF and XGBoost models, indicating that the GBoost model is more accurate in predicting the $M_w$ value than the RF and XGBoost models.

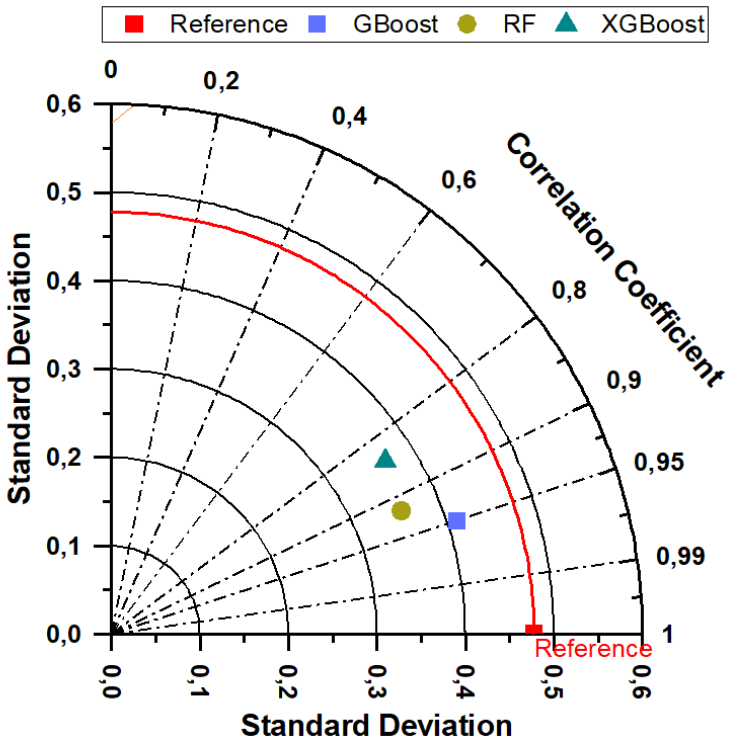



**Figure 7**. Illustration of Taylor diagram for the RF, GBoost, and XGBoost models.

### 5.4. Scaled percent error graph

In order to more comprehensively validate the predictive potential of the RF, GBoost and XGBoost models, *SPE* values were calculated using the following equation, as also used by Erzin [59], Erzin [61], and Erzin and Ecemis [74].

$$SPE = \frac{(\hat{y}_i - y_i)}{(y_{imax} - y_{imin})} \quad (5)$$

where $y_{i_{max}}$ and $y_{i_{min}}$ are the measured values' maximum and minimum values.

The *SPE* values calculated for the RF, GBoost and XGBoost models were then plotted against cumulative frequency in Fig. 8. Figure 8 shows that approximately 89.4%, 93.3% and 81.1% of the $M_w$ values predicted by the RF, GBoost and XGBoost models respectively are within ±10% of the *SPE*, indicating that the GBoost model performed better than the RF and XGBoost models in predicting the $M_w$ values.

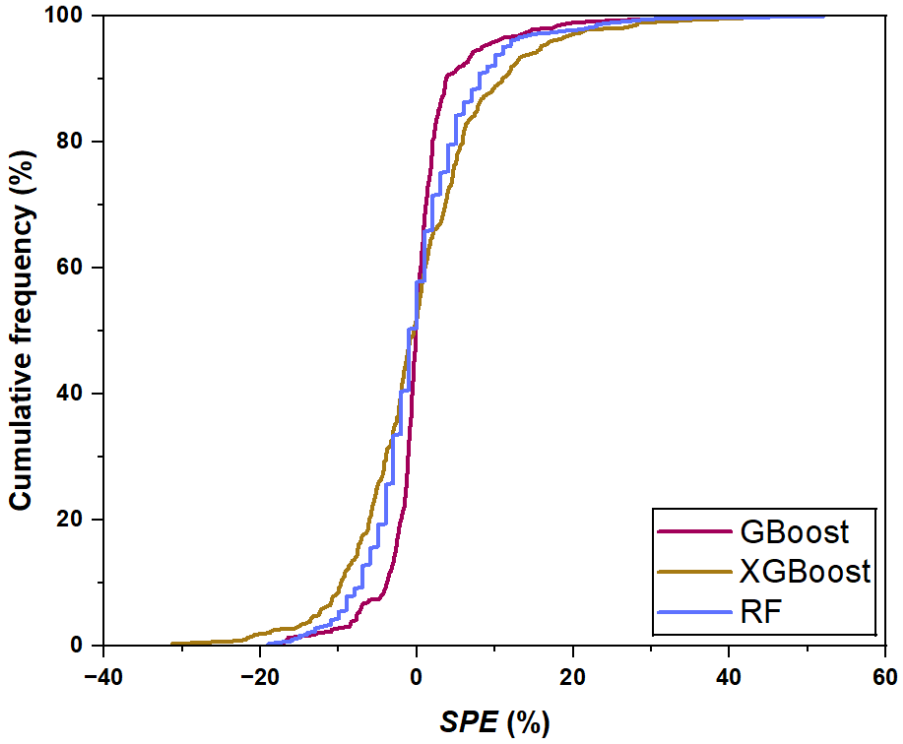



**Figure 8**. Cumulative frequency versus *SPE* for the RF, GBoost, and XGBoost models.

### 5.5. External validation

Golbraikh and Tropsha [75] established external validation criteria to evaluate and assess the performance or effectiveness of proposed ML models. These criteria establish if the suggested ML model is dependable, accurate, and compatible with the desired goals. The mathematical expressions used to calculate the validation parameters, and their conditions are given in Table 7. In Table 7, $k$ and $k'$ denote the slopes of the predicted vs. recorded $M_w$ and recorded vs. predicted $M_w$ with respect to the origin; $R_o^2$ and $R'^2_o$ represent the determination coefficient of the predicted vs. recorded $M_w$ and recorded vs. predicted $M_w$; $R_m$ is a confirmation indicator of the proposed ML models' external predictability; and $m$ and $n$ represent the factors for determining the proposed ML models' computational power.

**Table 7**. The mathematical expressions for the external validation parameters and their conditions.

| *Validation parameters* | Mathematical expression | Condition | Suggested by |
|---|---|---|---|
| $k$ | $k = \frac{\sum_{i=1}^{n}(y_i \times \hat{y}_i)}{\sum_{i=1}^{n} \hat{y}_i^2}$ | $0.85 \leq k \leq 1.15$ | Golbraikh and Tropsha [75] |
| $k'$ | $k' = \frac{\sum_{i=1}^{n}(y_i \times \hat{y}_i)}{\sum_{i=1}^{n} y_i^2}$ | $0.85 \leq k' \leq 1.15$ | Golbraikh and Tropsha [75] |
| $R_o^2$ | $R_o^2 = 1 - \frac{\sum_{i=1}^{n}(\hat{y}_i - k \times \hat{y}_i)^2}{\sum_{i=1}^{n}(\hat{y}_i - \bar{\hat{y}})^2}$ | Close to 1 | Alavi et al. [76] |
| $R'^2_o$ | $R'^2_o = 1 - \frac{\sum_{i=1}^{n}(y_i - k' \times y_i)^2}{\sum_{i=1}^{n}(y_i - \bar{y})^2}$ | Close to 1 | Alavi et al. [76] |
| $R_m$ | $R_m = R^2 \times \left(1 - \sqrt{\lvert R^2 - R_o^2 \rvert}\right)$ | $R_m > 0.5$ | Roy and Roy [77] |
| $m$ | $m = \frac{R^2 - R_o^2}{R^2}$ | $m < 0.1$ | Golbraikh and Tropsha [75] |
| $n$ | $n = \frac{R^2 - R'^2_o}{R^2}$ | $n < 0.1$ | Golbraikh and Tropsha [75] |

The RF, GBoost and XGBoost models developed are externally validated to evaluate their reliability and accuracy in predicting the $M_w$ value. Table 8 shows the values of the external validation parameters calculated for the developed RF, GBoost and XGBoost models. Table 8 shows that all the models developed meet all the conditions for external validation proposed by the investigators. In addition, as shown in Table 8, all three models meet all the requirements for external validation, indicating that they have strong validity, predictive power and more than just a correlation between output and input variables.

**Table 8**. External validation parameters for the RF, GBoost, and XGBoost models.

| **Model** | **External validation parameter** | | | | | | |
|---|---|---|---|---|---|---|---|
| | $k$ | $k'$ | $R_o^2$ | $R'^2_o$ | $R_m$ | $m$ | $n$ |
| **RF** | 1.015 | 0.972 | 0.995 | 0.990 | 0.892 | 0.009 | 0.004 |
| **GBoost** | 1.011 | 0.981 | 0.998 | 0.995 | 0.916 | -0.006 | -0.003 |
| **XGBoost** | 1.009 | 0.969 | 0.998 | 0.987 | 0.837 | -0.021 | -0.010 |

### 5.6. Sensivity analysis

Sensitivity analysis determines how effective input parameters are at predicting output parameter(s). This analysis can be used to determine the parameters that have the greatest influence on the prediction [78] It can also be used for the development of the most efficient AI models through the avoidance of input parameters which are insignificant [78]. Several researchers [78-82] have applied the cosine amplitude method for sensitivity analysis. The mathematical formula of the cosine amplitude method is presented in the following equation [83].

$$r_{ij}=\frac{\sum_{k=1}^{n} X_{ik} \times X_{jk}}{\sqrt{\sum_{k=1}^{n} X_{ik}^{2} \times \sum_{k=1}^{n} X_{jk}^{2}}} \quad (6)$$

where $n$ is the data values' number; $X_{ik}$ and $X_{jk}$ are the input and output parameters. $r_{ij}$ shows the strength of the relationship between each input parameter and the model output, and ranges between 0 and 1. This means that if the output parameter has no association with the input parameter, the $r_{ij}$ value is zero. A higher $r_{ij}$ value implies a greater influence of the input variable on the output parameter. The $r_{ij}$ values for all input parameters are presented in Fig. 9 for the RF, GBoost and XGBoost models. As shown in Fig. 9, the $r_{ij}$ values for all input parameters are higher than 0.5, indicating that all four input parameters affect the prediction of $M_w$ from the proposed RF, GBoost and XGBoost models, but with different effects. Figure 9 shows that $C_{Rn}$ with $r_{ij}$ values of 0.896, 0.872 and 0.911 for the RF, GBoost and XGBoost models rank the highest, indicating that $C_{Rn}$ has the most significant input parameter affecting the prediction of $M_w$ from the proposed RF, GBoost and XGBoost models. Figure 10 also shows that $T$ with $r_{ij}$ values of 0.671, 0.648 and 0.666 for the RF, GBoost and XGBoost models rank the lowest, indicating that $T$ has the least influence input parameter affecting the prediction of $M_w$ from the proposed RF, GBoost and XGBoost models.

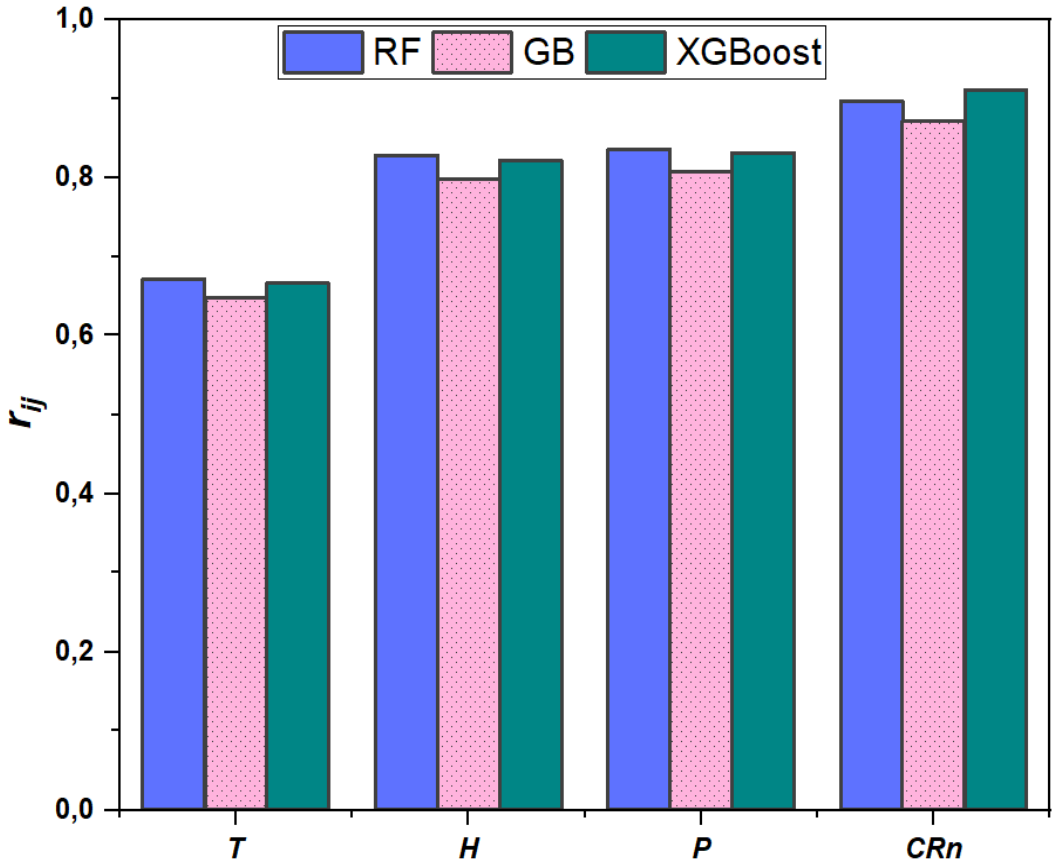



**Figure 9**. $r_{ij}$ values for all input parameters used in the RF, GBoost, and XGBoost models.

## 6. Conclusion

The current research evaluates the performance of the RF, GBoost and XGBoost models in predicting the $M_w$ value from soil gas $C_{Rn}$ and three meteorological parameters ($T$, $H$, and P). The RF, GBoost and XGBoost models were built using a total of 386 datasets including measured soil gas $C_{Rn}$ values and recorded $M_w$, $H$, $T$, and $P$ values. The *MAE*, *RMSE*, *RSR* and *RAE* statistics were then used to verify and evaluate the generated RF, GBoost and XGBoost models. The performance of the models was also confirmed by rank analysis and visually presented using Taylor and *SPE* plots. The research's crisp conclusions are the following:

• During the training and testing phases, all the RF, GBoost and XGBoost models produced a very strong correlation ($r > 0.8$) between predicted and recorded $M_w$ values, indicating that all the models predicted $M_w$ values more accurately.
• GBoost model gave smaller *MAE*, *RMSE*, *RSR* and *RAE* values than XGBoost and RF models for training and testing samples, demonstrating that the GBoost model outperformed XGBoost and RF models in predicting the $M_w$ value.
• The rank analysis of GBoost, XGBoost and RF models revealed that GBoost model had highest scores, signifying that GBoost model achieved better prediction accuracy in the prediction of the $M_w$ value than RF and XGBoost models
• Taylor and *SPE* graphs showed that GBoost model predicted the $M_w$ value more precisely than RF and XGBoost models.
• The $M_w$ value can be predicted reliably and quickly using the developed GBoost models, provided soil gas $C_{Rn}$ and three meteorological parameters ($H$, $T$, and $P$) are available.

## Declarations

The authors have read, understood, and have complied as applicable with the statement on "Ethical responsibilities of Authors" as found in the Instructions for Authors.

## Conflict of interest

The authors declare that there is no conflict of interest regarding the publication of this paper.

## Author contributions

**Selin Erzin**: Investigation, Conceptualization, Data curation, Validation, Methodology, Visualization, Supervision, Writing- original draft, Writing – review & editing

**Can Saç**: Measurement and collection of data.

## Funding

This study received no funding.

## Data availability

All datasets created during the current investigation are available upon reasonable request from the corresponding author.

## Consent to participate

This paper contains no studies involving human subjects conducted by any of the writers.

## References

**[1].** Jilani Z, Mehmood T, Alam A, Awais M, Iqbal T (2017) Monitoring and descriptive analysis of radon in relation to seismic activity of Northern Pakistan *Journal of Environmental Radioactivity*; 172:43-51.

**[2].** Asim KM, Martínez-Álvarez F, Basit A, Iqbal T (2017) Earthquake magnitude prediction in Hindukush region using machine learning techniques. *Natural Hazards*; 85:471-486.

**[3].** Martinelli G, Dadomo A (2017) Factors constraining the geographic distribution of earthquake geochemical and fluid-related precursors *Chemical Geology*; 469:176-184.

**[4].** Cothern C R, Smith JE (Eds.) (1987) Environmental radon (Vol. 35). Springer Science & Business Media.

**[5].** Wilkening M (1990) Radon in the Environment (Vol. 40). Elsevier.

**[6].** Reddy DV, Sukhija BS, Nagabhushanam P, Kumar D (2004) A clear case of radon anomaly associated with a micro-earthquake event in a Stable Continental Region. *Geophysical Research Letters;* 31(10).

**[7].** Moussa MM, El Arabi AGM (2003) Soil radon survey for tracing active fault: a case study along Qena-Safaga road, Eastern Desert, Egypt. *Radiation Measurements*; 37(3):211-216.

**[8].** Wakita H (1996) Geochemical challenge to earthquake prediction. *Proceedings of the National Academy of Sciences*; 93(9):3781-3786.

**[9].** Hartmann J, Levy JK (2005) Hydrogeological and gasgeochemical earthquake precursors–A review for application. *Natural Hazards*; 34:279-304.

**[10].** Singh S, Jaishi HP, Tiwari RP, Tiwari RC (2016) A study of variation in soil gas concentration associated with earthquakes near Indo-Burma Subduction zone. *Geoenvironmental Disasters*; 3:1-8.

**[11].** Zmazek B, Todorovski L, Džeroski S, Vaupotič J, Kobal I (2003) Application of decision trees to the analysis of soil radon data for earthquake prediction. *Applied Radiation and Isotopes*; 58(6):697-706.

**[12].** Walia V, Virk HS, Bajwa BS (2006) Radon precursory signals for some earthquakes of magnitude> 5 occurred in NW Himalaya: An overview. *Pure and Applied Geophysics*; 163:711-721.

**[13].** Iwata D, Nagahama H, Muto J, Yasuoka Y (2018) Non-parametric detection of atmospheric radon concentration anomalies related to earthquakes. *Scientific Reports*; 8: 3028.

**[14].** Kawabata K, Sato T, Takahashi HA, Tsunomori F, Hosono T, Takahashi M, Kitamura Y (2020) Changes in groundwater radon

concentrations caused by the 2016 Kumamoto earthquake. *Journal of Hydrology*; 584: 124712.

**[15].** Chowdhury S, Deb A, Barman C, Nurujjaman M, Bora DK (2022) Simultaneous monitoring of soil 222Rn in the Eastern Himalayas and the geothermal region of eastern India: an earthquake precursor. *Natural Hazards*;112: 1477–1502.

**[16].** Galiana-Merino JJ, Molina S, Kharazian A, Toader VE, Moldovan IA, Gomez I (2022) Analysis of radon measurements in relation to daily seismic activity rates in the vrancea region, romania. *Sensors*; 22: 4160.

**[17].** Karastathis VK, Eleftheriou G, Kafatos M, Tsinganos K, Tselentis GA, Mouzakiotis E, Ouzounov D (2022) Observations on the stress related variations of soil radon concentration in the Gulf of Corinth, Greece *Scientific Reports*;12: 5442.

**[18].** Manisa K, Erdogan M, Zedef V, Bircan H, Bicer A (2022) Variations of 222Rn concentrations over active fault system in Simav, Kutahya, Western Turkey: Possible causes for soil-gas 222Rn anomalies. *Applied Radiation Isotopes* ;190: 110484.

**[19].** Alam A, Nikolopoulos D, Wang N (2023) Fractal Patterns in Groundwater Radon Disturbances Prior to the Great 7.9 Mw Wenchuan Earthquake, China. *Geosciences*;13(9):268.

**[20].** Jaishi HP, Singh S, Tiwari RP, Tiwari RC (2023) Analysis of Subsurface Soil Radon with the Environmental Parameters and Its Relation with Seismic Events. *Journal of the Geological Society of India*; 99: 847–858.

**[21].** Romano D, Sabatino G, Magazù S, Di Bella M, Tripodo A, Gattuso A, Italiano F (2023). Distribution of soil gas radon concentration in north-eastern Sicily (Italy): hazard evaluation and tectonic implications. *Environmental Earth Sciences*; 82(11): 273.

**[22].** Walia V, Kumar A, Chowdhury S, Lin SJ, Lee HF, Fu CC (2024) Earthquake precursory study using decomposition technique: time series soil radon monitoring data from the San-Jie Station in Northern Taiwan. *Journal of Radioanalytical and Nuclear Chemistry*; 333(6): 3047-3054.

**[23].** Baykut S, Akgül T, İnan S, Seyis C (2010) Observation and removal of daily quasi-periodic components in soil radon data. *Radiation Measurements*; 45(7):872-879.

**[24].** Oh Y, Kim G (2015) A radon-thoron isotope pair as a reliable earthquake precursor. *Scientific Reports*; 5:13084.

**[25].** Saç MM, Harmansah C, Camgoz B, Sozbilir H (2011) Radon monitoring as the earthquake precursor in fault line in Western Turkey. *Ekoloji*; 20(79):93-98.

**[26].** Yang TF, Walia V, Chyi LL, Fu CC, Chen CH, Liu TK, ... Lee M (2005) Variations of soil radon and thoron concentrations in a fault zone and prospective earthquakes in SW Taiwan. *Radiation Measurements*; 40(2-6): 496-502.

**[27].** Friedman JH (2001) Greedy function approximation: a gradient boosting machine. *Annals of Statistics*; 1189-1232.

**[28].** Huang S (2024) Processing and Comparison of GBoost, XGBoost, and Random Forest in Titanic Survival Prediction. *Applied and Computational Engineering*; 102:175-182.

**[29].** Chen T, Guestrin C (2016) Xgboost: A scalable tree boosting system. In Proceedings of the 22nd ACM SIGKDD International Conference on Knowledge Discovery and Data Mining (pp. 785-794).

**[30].** Breiman L (2001) Random forests. *Machine Learning*; 45:5-32.

**[31].** AFAD (2021) Disaster and Emergency Management, (n.d.). http://www.afad.gov.tr

**[32].** TEC (2018) Turkish Earthquake Code: Specifications for Building Design Under Earthquake Effects, Regulations on structures constructed in disaster regions, Ankara

**[33].** Freund Y, Schapire R, Abe N (1999) A short introduction to boosting. *Journal-Japanese Society for Artificial Intelligence*; 14(5):771-780.

**[34].** Persson C, Bacher P, Shiga T, Madsen H (2017) Multi-site solar power forecasting using gradient boosted regression trees. *Solar Energy*; 150:423-436.

**[35].** Wang FK, Mamo T (2020) Gradient boosted regression model for the degradation analysis of prismatic cells. *Computers & Industrial Engineering*; 144:106494.

**[36].** Kumar P, Alruqi M, Hanafi HA, Sharma P, Wanatasanappan VV (2024) Effect of particle size on second law of thermodynamics analysis of Al2O3 nanofluid: application of XGBoost and gradient boosting regression for prognostic analysis. *International Journal of Thermal Sciences*; 197:108825.

**[37].** Pathy A, Meher S (2020) Predicting algal biochar yield using eXtreme Gradient Boosting (XGB) algorithm of machine learning methods. *Algal Research*; 50:102006.

**[38].** Qiu Y, Zhou J, Khandelwal M, Yang H, Yang P, Li C (2022) Performance evaluation of hybrid WOA-XGBoost, GWO-XGBoost and BO-XGBoost models to predict blast-induced ground vibration. *Engineering with Computers*; 38(5):4145-4162.

**[39].** Kumar D, Sood SK, Rawat KS (2023) Early health prediction framework using XGBoost ensemble algorithm in intelligent environment. *Artificial Intelligence Review*; 56(1):1591-1615.

**[40].** Li X, Ma L, Chen P, Xu H, Xing Q, Yan J, ... Cheng Y (2022) Probabilistic solar irradiance forecasting based on XGBoost. *Energy Reports*; 8:1087-1095.

**[41].** Sagi O, Rokach L (2021) Approximating XGBoost with an interpretable decision tree. *Information Sciences*; 572: 522-542.

**[42].** Zhang P, Jia Y, Shang Y (2022) Research and application of XGBoost in imbalanced data. *International Journal of Distributed Sensor Networks*; 18(6):15501329221106935.

**[43].** Sahin EK, Colkesen I, Kavzoglu T (2020) A comparative assessment of canonical correlation forest, random forest, rotation forest and logistic regression methods for landslide susceptibility mapping. *Geocarto International*; 35(4):341-363.

**[44].** Wu Y, Liu H, Liu S, Lou C (2023) Estimate of near-surface NO2 concentrations in Fenwei Plain, China, based on TROPOMI data and random forest model. *Environmental Monitoring and Assessment*; 195(11):1379.

**[45].** Khan M, Khan A U, Houda M, El Hachem C, Rasheed M, Anwar W (2023) Optimizing durability assessment: Machine learning models for depth of wear of environmentally-friendly concrete. *Results in Engineering*; 20:101625.

**[46].** Sharma C, Ojha CSP (2019) Statistical parameters of hydrometeorological variables: standard deviation, SNR, skewness and kurtosis. In Advances in Water Resources Engineering and Management:select proceedings of TRACE 2018 (pp. 59-70). Singapore: Springer Singapore.

**[47].** Cain MK, Zhang Z, Yuan KH (2017) Univariate and multivariate skewness and kurtosis for measuring nonnormality: Prevalence, influence, and estimation. *Behavior Research Methods*; 49: 1716-1735.

**[48].** Benson CH (1993) Probability distributions for hydraulic conductivity of compacted soil liners. *Journal of Geotechnical Engineering*; 119(3):471-486.

**[49].** Brown SC, Greene JA (2006) The wisdom development scale: Translating the conceptual to the concrete. *Journal of College Student Development;* 47(1):1-19.

**[50].** Bulmer MG (1979) Principles of Statistics. Dover.

**[51].** Tabachnick BG, Fidell LS (2013) Using Multivariate Statistics. Pearson.

**[52].** Gravetter F, Wallnau L (2014) Essentials of statistics for the behavioral sciences. Wadsworth.

**[53].** Byrne BM, Van de Vijver FJ (2010) Testing for measurement and structural equivalence in large-scale cross-cultural studies: Addressing the issue of nonequivalence. *International Journal of Testing*; 10(2):107-132.

**[54]**. Hair Jr JF, Black WC, Babin BJ, Anderson RE (2010) Multivariate data analysis. In Multivariate Data Analysis (pp. 785-785).

**[55].** Hair Jr J, Wolfinbarger MC, Ortinau DJ, Bush RP (2013) Essentials of Marketing, New York, Mc Graw Hill.

**[56].** Rabbani A, Samui P, Kumari S (2023c) Optimized ANN-based approach for estimation of shear strength of soil. *Asian Journal of Civil Engineering;* 24(8):3627-3640.

**[57].** Nafouanti MB, Li J, Mustapha NA, Uwamungu P, Al-Alimi D (2021) Prediction on the fluoride contamination in groundwater at the Datong Basin, Northern China: comparison of random forest, logistic regression and artificial neural network. A*pplied Geochemistry*; 132:105054.

**[58].** Erzin S (2024a) Using radial basis artificial neural networks to predict radiation hazard indices in geological materials. *Environmental Monitoring and Assessment*; 196(3):315.

**[59].** Erzin S (2024b) Prediction of the radon concentration in thermal waters using artificial neural networks. *International Journal of Environmental Science and Technology*; 21(10):7321-7328.

**[60].** Erzin S (2025) Optimization of artificial neural network for predicting radon exhalation rates and effective radium content in soil samples. *Earth Science Informatics*; 18(1):170.

**[61].** Erzin S, Yaprak G (2022) Prediction of the activity concentrations of 232Th, 238U and 40K in geological materials using radial basis function neural network. *Journal of Radioanalytical and Nuclear Chemistry*; 331(9):3525-3533.

**[62].** Rabbani A, Samui P, Kumari S (2023a) A novel hybrid model of augmented grey wolf optimizer and artificial neural network for predicting shear strength of soil. *Modeling Earth Systems and Environment*; 9(2):2327-2347.

**[63].** Rabbani A, Samui P, Kumari S (2023b) Implementing ensemble learning models for the prediction of shear strength of soil. *Asian Journal of Civil Engineering*; 24(7):2103-2119.

**[64].** Santos-Pereira J, Gruenwald L, Bernardino J (2022) Top data mining tools for the healthcare industry. *Journal of King Saud University-Computer and Information Sciences*; 34(8):4968-4982.

**[65].** Thornton C, Hutter F, Hoos HH, Leyton-Brown K (2013) Auto-WEKA: Combined selection and hyperparameter optimization of classification algorithms. In Proceedings of the 19th ACM SIGKDD International Conference on Knowledge Discovery and Data Mining (pp. 847-855).

**[66].** DeCastro-García N, Muñoz Castañeda ÁL, Escudero García D, Carriegos MV (2019) Effect of the sampling of a dataset in the hyperparameter optimization phase over the efficiency of a machine learning algorithm. *Complexity*; 1:6278908.

**[67].** Belete D M, Huchaiah M D (2022) Grid search in hyperparameter optimization of machine learning models for prediction of HIV/AIDS test results. *International Journal of Computers and Applications*; 44(9):875-886.

**[68].** Zöller MA, Huber MF (2021) Benchmark and survey of automated machine learning frameworks. *Journal of Artificial Intelligence Research*; 70:409-472.

**[69].** Khatti J, Grover KS (2024) Assessment of hydraulic conductivity of compacted clayey soil using artificial neural network: An investigation on structural and database multicollinearity. *Earth Science Informatics*; 17(4): 3287-3332.

**[70].** Khatti J, Grover KS, Kim HJ, Mawuntu KBA, Park TW (2024) Prediction of ultimate bearing capacity of shallow foundations on cohesionless soil using hybrid LSTM and RVM approaches: An extended investigation of multicollinearity. *Computers and Geotechnics*; 165:105912.

**[71]**. Rabbani A, Samui P, Kumari S, Saraswat BK, Tiwari M, Rai A (2024) Optimization of an artificial neural network using three novel meta-heuristic algorithms for predicting the shear strength of soil. *Transportation Infrastructure Geotechnology*; 11(4):1708-1729.

**[72].** Kumar M, Kumar DR, Khatti J, Samui P, Grover KS (2024b) Prediction of bearing capacity of pile foundation using deep learning approaches. *Frontiers of Structural and Civil Engineering*; 18(6):870-886.

**[73].** Biswas R, Kumar M, Singh RK, Alzara M, El Sayed SBA, Abdelmongy M, ... Yousef SEA (2023) A novel integrated approach of RUNge Kutta optimizer and ANN for estimating compressive strength of self-compacting concrete. *Case Studies in Construction Materials*; 18: e02163.

**[74].** Erzin Y, Ecemis N (2017) The use of neural networks for the prediction of cone penetration resistance of silty sands. *Neural Computing Applications*; 28:727-736.

**[75].** Golbraikh A, Tropsha A (2002) Beware of q2!. *Journal of Molecular Graphics and Modelling*; 20(4):269-276.

**[76].** Alavi AH, Ameri M, Gandomi AH, Mirzahosseini MR (2011) Formulation of flow number of asphalt mixes using a hybrid computational method. *Construction and Building Materials*; 25(3):1338-1355.

**[77].** Roy PP, Roy K (2008) On some aspects of variable selection for partial least squares regression models. *QSAR & Combinatorial Science*; 27(3):302-313.

**[78].** Khatti J, Grover KS (2023) Prediction of compaction parameters for fine-grained soil: Critical comparison of the deep learning and standalone models. *Journal of Rock Mechanics and Geotechnical Engineering*; 15(11):3010-3038.

**[79].** Ardakani A, Kordnaeij A (2019) Soil compaction parameters prediction using GMDH-type neural network and genetic algorithm. *European Journal of Environmental and Civil Engineering*; 23(4):449-462.

**[80].** Chen W, Hasanipanah M, Nikafshan Rad H, Jahed Armaghani D, Tahir MM (2021) A new design of evolutionary hybrid optimization of SVR model in predicting the blast-induced ground vibration. *Engineering with Computers*; 37:1455-1471.

**[81].** Shirani Faradonbeh R, Jahed Armaghani D, Abd Majid MZ, Md Tahir M, Ramesh Murlidhar B, Monjezi M, Wong HM (2016) Prediction of ground vibration due to quarry blasting based on gene expression programming: a new model for peak particle velocity prediction. *International Journal of Environmental Science and Technology;* 13:1453-1464.

**[82].** Wang HL, Yin ZY (2020) High performance prediction of soil compaction parameters using multi expression programming. *Engineering Geology*; 276:105758.

**[83].** Momeni E, Nazir R, Armaghani DJ, Maziar H (2014) Prediction of pile bearing capacity using a hybrid genetic algorithm-based ANN. *Measurement*; 57:122-131.